2014 International Conference on Unmanned Aircraft Systems (ICUAS)
May 27-30, 2014. Orlando, FL, USA

# Nonlinear observers applied to fixed-wing UAVs

P. Parada[1],T. Espinoza[1], A. Dzul[1]

*Abstract*— **This paper presents a comparison of two types of robust observers algorithms: the sliding-mode observer (SMO) and the nonlinear extended state observer (NESO). For some controllers design, it is necessary the use of observers in order to estimate the states which are not directly available. We present several simulations for the sliding-mode observer and the nonlinear extended state observer. In order to validate the robustness of such observers, we have developed a fixed-wing UAV platform, and we have designed a Proportional-Derivative (PD) control law which uses the output signals of the observer as state feedback. The analyzed movements are the altitude, roll and yaw.**

**Keywords: sliding mode observers, nonlinear extended state observer, airplane model, fixed-wing UAV.**

## I. INTRODUCTION

The work developed by Luenberger in [1] has proven the usefulness of the state observers. They are a powerful tool when we have not access to some states signals. The state observers have been employed in monitoring, control and even on the detection and identification of failures in dynamical systems. Since almost all observer designs are based on the mathematical model of the plant, the presence of disturbances, dynamic uncertainties, and nonlinearities pose great challenges in practical applications. By the above, the high-performance robust observer design problem has been a topic of considerable interest, and several advanced observer designs have been proposed [2]. The sliding-mode observers (SMO) potentially offer advantages similar to those of sliding-mode controllers, in particular, inherent robustness to parametric uncertainty, and they are easy to implement in certain nonlinear systems. Further, contrary to the case of controller design, chattering issues in sliding-mode observer design are only linked to numerical implementation [3]. The earlier work was introduced by Slotine [3] and Utkin [4]. We can cite, besides others, the next papers which use the SMO: R. Sreedhar [5] has used the SMO for robust fault detection in nonlinear systems; F. J. J. Hermans and M. B. Zarrop [6] have presented robust sensor monitoring using SMO; G. Foo and M. F. Rahman [7] use the SMO in a sliding-mode MTPA control of an IPM synchronous motor drive, etc.

A class of nonlinear extended state observers (NESO) was proposed by J. Han [8] in 1995. It is rather independent of mathematical model of the plants, thus achieving inherent robustness. It was tested and verified in key industrial control problems, for example in [9], [10].

In the last years, the fixed-wing UAV systems have had a large number of applications, for example: monitoring disaster areas, localization of victims, infrastructure inspection for inaccessible locations, tasks of surveillance and photography [11]. Since such aerial systems can present sensor failures, or simply, its avionics must be lighter, then we need algorithms that can guarantee the availability of all states signals for control purposes. By this fact, in this paper we present a comparative analysis (simulation results) of the SMO and the NESO when they are applied to the dynamic model of a fixed-wing UAV. The comparison criteria are based on the observer tracking errors and the performance robustness with respect to the plant uncertainties. We show that the SMO presents a better performance with respect to the NESO. Concerning the experimental results, we have only validated the SMO, due to the final paper deadline. The estimated states have been used as feedback signals for Proportional-Derivative (PD) control laws applied to the roll, yaw and altitude movements.

The organization of the paper is as follows. Section II presents the mathematical model of the

[1]Pavel Parada, Tadeo Espinoza and Alejandro Dzul are with División de Estudios de Posgrado e Investigación, Instituto Tecnológico de la Laguna, 27000 Torreón, Coahuila, México dzul@faraday.itlalaguna.edu.mx

airplane. The section III deals with the design of the state observers, and the section IV shows the PD control design. In section V, it is shown the simulation results of the PD controller with the SMO and NESO observers applied to the dynamic model of a fixed-wing UAV. The fixed-wing UAV platform and the experimental results are presented in section VI. Conclusions and the future work are presented in section VII.

## II. Airplane Model

In this section, we present the dynamic model of an airplane. The next equations describe the longitudinal and lateral dynamics. Several considerations have been taken into account in order to obtain these dynamic models [12], [13].

### A. Longitudinal dynamics

The parameters which are involved in the longitudinal dynamic model (1)-(5) are shown in Figure 1. These parameters allow to analyzing the movement toward the front of an airplane [13], particularly the altitude control.

$$\dot{\theta} = q \quad (1)$$

$$\dot{q} = \frac{M}{I_{yy}} \quad (2)$$

$$\dot{h} = V \sin\theta \quad (3)$$

$$\dot{V} = \frac{1}{m}\left(-D + T\cos\alpha - mg\sin\gamma\right) \quad (4)$$

$$\dot{\gamma} = \frac{1}{mV}\left(L + T\sin\alpha - mg\sin\gamma\right) \quad (5)$$

where $V$ is the relative speed of the aircraft, $\alpha$ describes the angle of attack, $\gamma$ represents the flight-path angle and $\theta$ denotes the pitch angle. In addition, $q$ is the pitch angular rate (with respect to the $y$-axis of the aircraft body), $T$ denotes the force of engine thrust, $h$ is the airplane altitude [13] and $\delta_e$ represents the elevator deviation where the control action is applied. The aerodynamic effects on the airplane are obtained by the lift force $L$ and the drag force $D$. $M$ is the pitching moment which acts on the airplane, $m$ denotes the total mass of the airplane, $g$ is the gravitational constant and $I_{yy}$ describes the component $y$ of the diagonal of the inertia matrix in the fixed frame of the aircraft. The value of angle of attack is obtained by using the following relation $\alpha = \theta - \gamma$ [14]. The lift force $L$, the drag force $D$, and the pitching moment $M$ are defined as [13]:

$$L = \bar{q}SC_L \quad (6)$$

$$D = \bar{q}SC_D \quad (7)$$

$$M = \bar{q}S\bar{c}C_M \quad (8)$$

where $\bar{q}$ denotes the aerodynamic pressure. $S$ represents the wing platform area and $\bar{c}$ is the mean aerodynamic chord. $C_D$, $C_L$ and $C_M$ are the aerodynamics coefficients for drag force, lift force and pitch moment respectively.

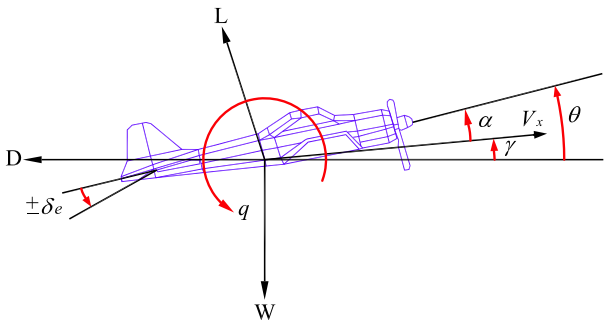


Fig. 1. Pure pitching motion

### B. Lateral dynamics

The lateral dynamics generates the roll motion and, at the same time, induces a yaw motion (and vice versa), then a natural coupling exists between the rotations about the axes of roll and yaw [16]. In our case, to solve it, we have considered that there is a decoupling of yaw and roll movements [15]. Thus, each movement can be controlled independently. Generally, the effects of the engine thrust are also ignored [16], that is, we are only interested in the angular motions. In the Figure 2, the yaw motion is represented and it can be described by the following equations:

$$\dot{\psi} = r \quad (9)$$

$$\dot{r} = \frac{N}{I_{zz}} \quad (10)$$

$$\dot{V}_y = \frac{F_y}{m} - rV_x \quad (11)$$

$$\dot{V}_x = \frac{F_x}{m} + rV_y \quad (12)$$

where $\psi$ represents the angle of yaw and $r$ denotes the yaw rate, with respect to the center of gravity of the airplane, $N$ is the yawing moment and $I_{zz}$

represents the inertia in the $z$-axis in the fixed frame of the aircraft. The control law is applied in $\delta_r$ that is the rudder deflection. $V_x$ corresponds to the speed of the airplane in the longitudinal $x$-axis, $V_y$ is the speed in the lateral $y$-axis, $F_x$ describes the thrust force in the longitudinal $x$-axis and $F_y$ denotes the component of the resultant lateral force on the $y$-axis. The equations related to the above forces and the yaw moment are [14]:

$$F_x = \bar{q}SC_{x0} \quad (13)$$
$$F_y = \bar{q}SC_y \quad (14)$$
$$N = \bar{q}SC_n \quad (15)$$

where $C_{x0}$, $C_y$ and $C_n$ are the aerodynamics coefficients which are involved for the lateral dynamics. These coefficients are obtained by considering small angles motions and with a low airplane speed. The following equations describe the dynamics for the roll motion:

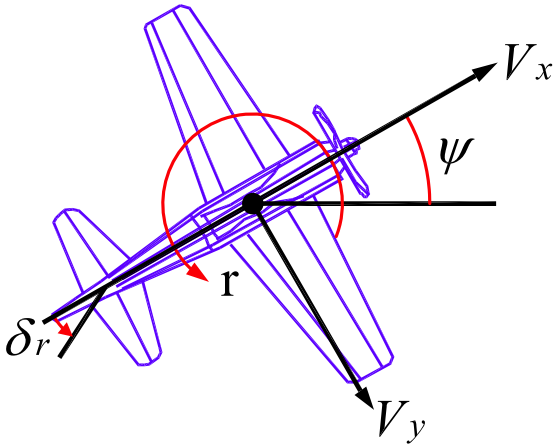


Fig. 2. Pure yawing motion

$$\dot{\phi} = p \quad (16)$$
$$\dot{p} = \frac{\bar{L}}{I_{xx}} \quad (17)$$
$$\dot{V}_y = \frac{F_y}{m} + pV_x \quad (18)$$
$$\dot{V}_x = \frac{F_x}{m} - pV_y \quad (19)$$

where $p$ denotes the roll rate, $\bar{L}$ is the rolling moment, $I_{xx}$ represents the inertia for the $x$-axis in the fixed frame of the aircraft and $\phi$ describes the roll angle. In the Figure 3, it is observed that $\delta_a$ represents the deviation of the ailerons, that is, it represents the input control signal. In the case of the roll moment, this corresponds to the expression $\bar{L} = \bar{q}SbC_L$, where $b$ is the wing span of the airplane and $C_L$ represents the aerodynamic coefficient of the roll moment [14].

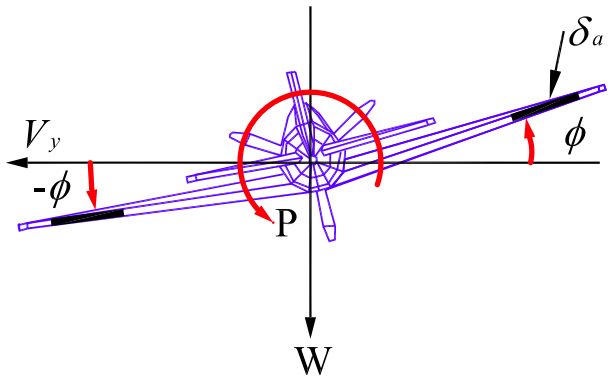


Fig. 3. Pure rolling motion

## III. Design of the State Observers

In this section, we describe the techniques for the design of the sliding-mode observer (SMO) and the nonlinear extended state observer (NESO).

### A. The Sliding-mode Observer

Let us now consider the system

$$\ddot{x} = f \quad (20)$$

where $f$ is a nonlinear function, with uncertain of the state $x$. The sliding-mode observer (SMO) for the nonlinear system (20) is defined by [3]:

$$\dot{\hat{x}}_1 = -\alpha_1\tilde{x}_1 + \hat{x}_2 - k_1\text{sgn}(\tilde{x}_1)$$
$$\dot{\hat{x}}_2 = -\alpha_2\tilde{x}_1 + \hat{f} - k_2\text{sgn}(\tilde{x}_1)$$

where $\tilde{x}_1 = \hat{x}_1 - x_1$ is the estimation error of the estimated variable $\hat{x}_1$ and the current $x_1$. The constants $\alpha_1$ and $\alpha_2$ are chosen to place the poles of the linearized system at desired locations. $k_1$ and $k_2$ are positive gains values, and $\text{sgn}(\cdot)$ is a *sign* function defined in [3].

### B. Nonlinear Extended State Observer

The previous observer depends on the knowledge of the dynamic model (20). The nonlinear extended states observers (NESO) [8] are an alternative method when we do not want to depend on the dynamic model. Consider (20) as an augmented equations system having the next form:

$$\left.\begin{aligned} \dot{x}_1 &= x_2 \\ \dot{x}_2 &= x_3 + b_0 u \\ \dot{x}_3 &= h \\ y &= x_1 \end{aligned}\right\} \tag{21}$$

where $f$ is taken as an extended state, $x_3$. For this observer, both $f$ and its derivative $\dot{f}$ are assumed unknown. In [8], it is proposed a nonlinear observer as

$$\left.\begin{aligned} \dot{\hat{x}}_1 &= \hat{x}_2 - \beta_1 g_1(e) \\ \dot{\hat{x}}_2 &= \hat{x}_3 - \beta_2 g_2(e) + b_0 u \\ \dot{\hat{x}}_3 &= -\beta_3 g_3(e) \end{aligned}\right\} \tag{22}$$

where $e = \hat{x}_1 - y$, $\hat{x}_3$ is the estimate of the uncertain function $f$. $\beta_1$, $\beta_2$ and $\beta_3$ are the observer gains. The function $g_i(\cdot)$ is defined as a modified exponential gain function

$$g_i(e, \alpha_i, \delta) = \begin{cases} |e|^{\alpha_i} \operatorname{sgn}(e), & |e| > \delta > 0 \\ \frac{e}{\delta^{1-\alpha_i}}, & |e| \leq \delta \end{cases} \tag{23}$$

Given that $\alpha$, in (23), is chosen between 0 and 1, the function $g_i(e, \alpha_i, \delta)$ yields a high gain value in the neighborhood of origin.

## IV. Controller Design

We have designed a PD control law (by the simplicity of the controller design) in order to analyse the behavior of the SMO and the NESO. The estimated states are used inside the controller algorithm.

For the case of the altitude control law design, we consider the equations which define the longitudinal dynamics, except the equation (4) which defines the linear longitudinal velocity, because it is considered as a constant velocity. We also define the error as $e_h = h_d - h$ in order to design the PD control, and it denotes the difference between the desired altitude $h_d$ with respect to the current altitude $h$. The control signal for the PD is given by

$$u = k_{pl}(e_h) + k_{vl}(\dot{e}_h) \tag{24}$$

where $k_{pl}$ and $k_{vl}$ are the control gains related to the PD control [17], [18]. $l$ denotes $h$, $\psi$ or $\phi$ if we consider the altitude, the yaw or the roll motions. For yaw and roll motions we have used the general structure shown in (24), but now, obviously it is considered that the errors are $e_\psi = \psi_d - \psi$ and $e_\phi = \phi_d - \phi$ respectively, where $\psi_d$ denotes the desired yaw angle and $\psi$ is obtained by integrating (9). $\phi_d$ is the desired roll angle and $\phi$ is obtained by integrating the roll rate in equation (16).

## V. Simulation Results

This section presents the simulation results that we have obtained for each one of the cases under analysis. The simulations include a white noise parameter on the output of the system in order to obtain results close to a real flight of a fixed-wing UAV.

The values of the proportional-derivative control law and state observers gains are shown in Table I. In the case of the NESO: $\alpha_i = \{1, 0.5, 0.25\}$ and $\delta = 10^{-3}$ for the three movements.

| Yaw | $k_{p\psi}$ | $k_{v\psi}$ | $k_1$ | $k_2$ | $\alpha_1$ | $\alpha_2$ | $\beta_1$ | $\beta_2$ | $\beta_3$ |
|---|---|---|---|---|---|---|---|---|---|
| SMO | 0.25 | 0.025 | 0.001 | 0.0001 | 8 | 10 | - | - | - |
| NESO | 0.25 | 0.025 | - | - | - | - | 28 | 180 | 180 |
| Roll | $k_{p\phi}$ | $k_{v\phi}$ | $k_1$ | $k_2$ | $\alpha_1$ | $\alpha_2$ | $\beta_1$ | $\beta_2$ | $\beta_3$ |
| SMO | 2 | 0.7 | 0.001 | 0.001 | 8 | 10 | - | - | - |
| NESO | 2 | 0.7 | - | - | - | - | 10 | 12 | 15 |
| Pitch | $k_{ph}$ | $k_{vh}$ | $k_1$ | $k_2$ | $\alpha_1$ | $\alpha_2$ | $\beta_1$ | $\beta_2$ | $\beta_3$ |
| SMO | 5 | 2 | 0.01 | 0.001 | 17 | 75 | - | - | - |
| NESO | 5 | 2 | - | - | - | - | 1.5 | 0.5 | 0.05 |

TABLE I
SIMULATION GAINS

### A. Yaw movement

The simulation results have been performed with an initial condition of 10 degrees, and the PD control target will be reached when the output of the dynamic system is stabilized at 0 degrees. Figure 4 shows the simulation results for yaw movement.

We can see that the PD control law, with SMO or NESO, achieves the desired value. The behavior of the yaw rate is presented in Figure 5, where the SMO has a better performance than NESO. The estimation error for yaw angle, applying SMO, is shown in Figure 6(a), and the estimation error for the NESO is observed in Figure 6(b). The estimation errors for yaw rate, with NESO or SMO, are shown in Figure 7(a) and 7(b) respectively.

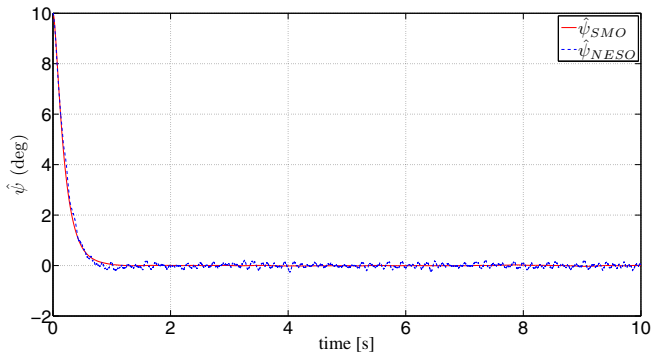


Fig. 4. Yaw motion behavior when is applied a PD with SMO or NESO

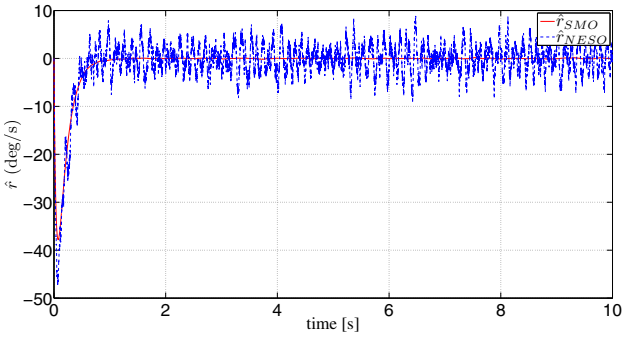


Fig. 5. Behavior of the yaw rate when applied SMO or NESO

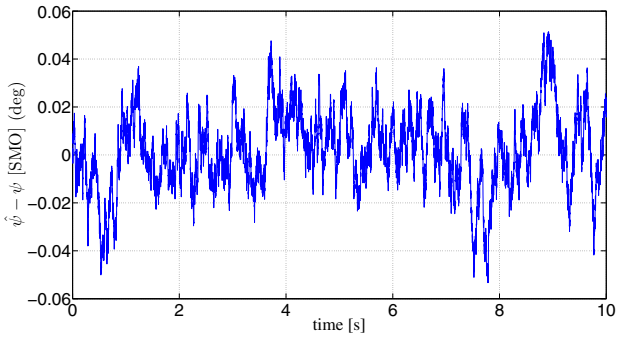


(a)

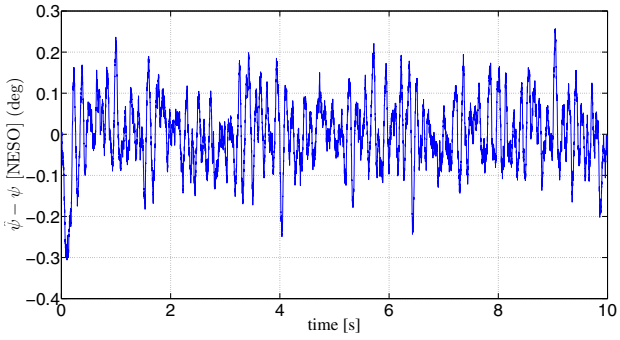


(b)

Fig. 6. Estimation error for the yaw angle. (a) Estimation error with SMO (b) Estimation error with NESO

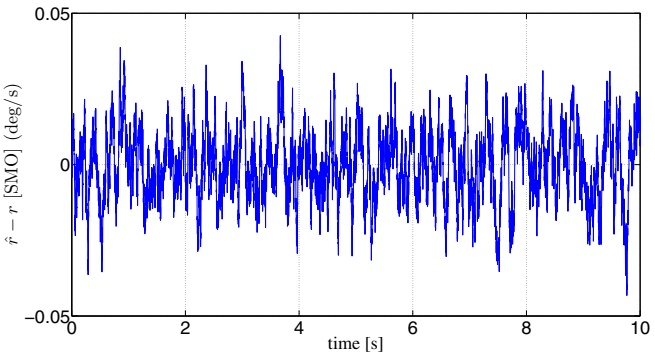


(a)

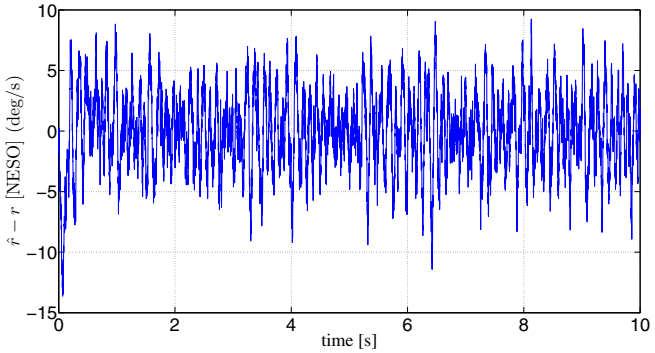


(b)

Fig. 7. Estimation error for yaw rate. (a) Estimation error with SMO (b) Estimation error with NESO

## *B. Roll movement*

Concerning the simulation of the roll motion, we have applied the same desired signal that has been used in the yaw motion, that is, with 10 degrees as the initial condition and with a control target in zero degrees, Figure 8. The Figure 9 shows the response of the roll rate when applying SMO or NESO. The estimation errors of the states for the roll angle are shown in Figures 10 and 11.

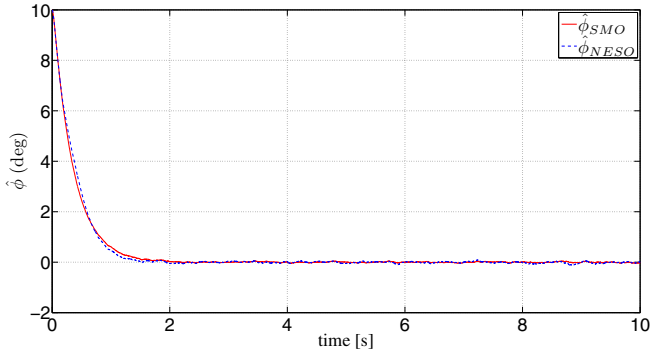


Fig. 8. Roll motion behavior when is applied a PD with SMO or NESO

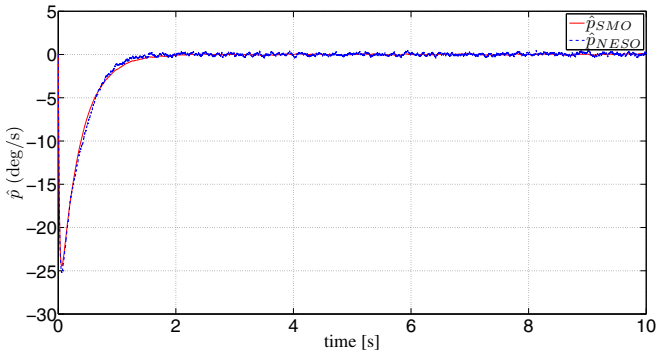


Fig. 9. Response of the roll rate with SMO or NESO

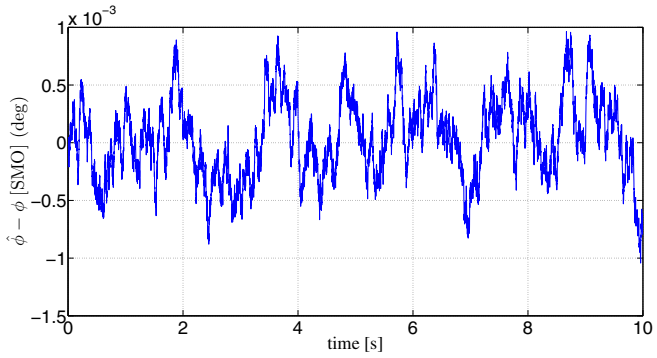


(a)

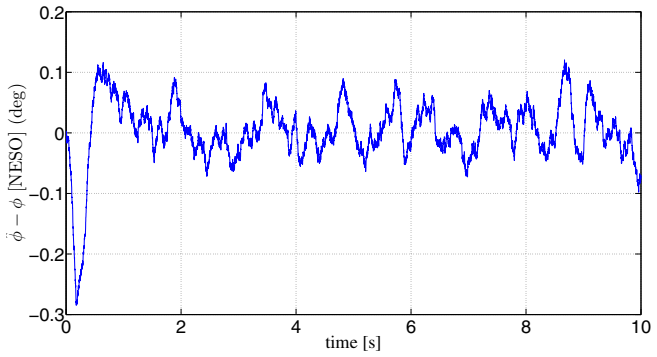


(b)

Fig. 10. Estimation errors for roll angle. (a) Estimation error with SMO (b) Estimation error with NESO

## C. Altitude movement

For this dynamics, it is considered that the fixed-wing UAV looking for achieve a desired altitude of 5 meters. The PD control law is applied on pitch angle in order to achieve the altitude error to zero. The simulation results of the pitch dynamics are shown in Figure 12. The Figures 13 and 14 show the responses of the estimated states of pitch movement and pitch rate, respectively. Estimation

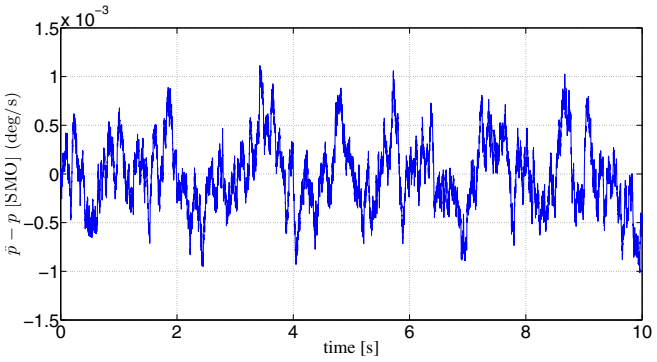


(a)

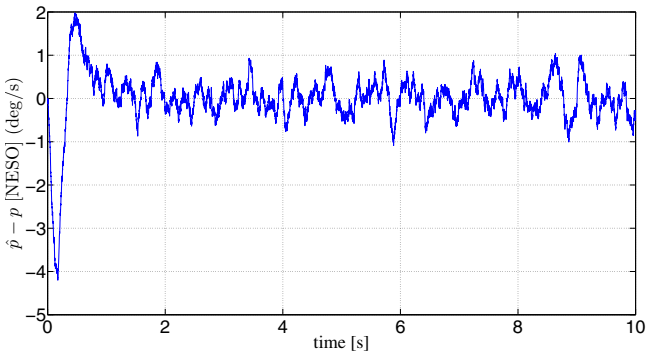


(b)

Fig. 11. Estimation errors for roll rate. (a) Estimation error with SMO (b) Estimation error with NESO

errors for SMO are shown in the Figure 15, and for NESO are show in the Figure 16.

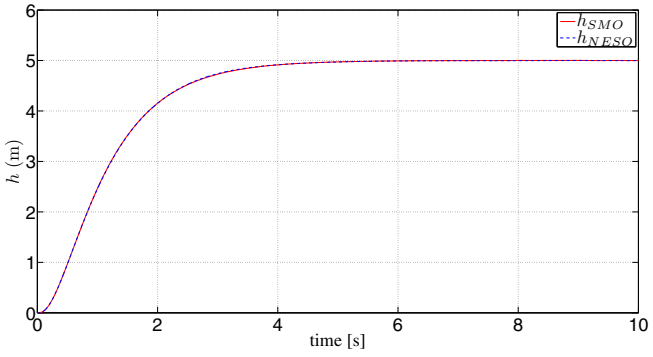


Fig. 12. Altitude motion behavior when is applied a PD with SMO or NESO

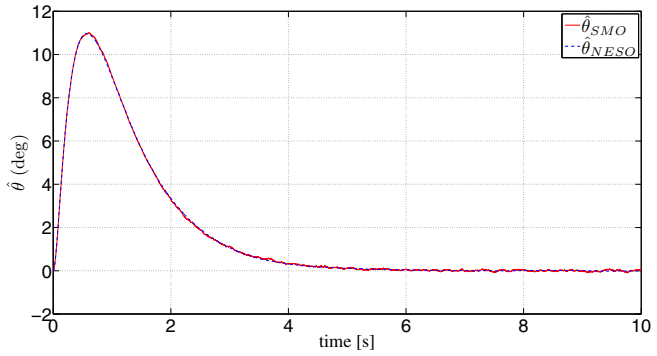


Fig. 13. Response of the pitch angle with SMO or NESO

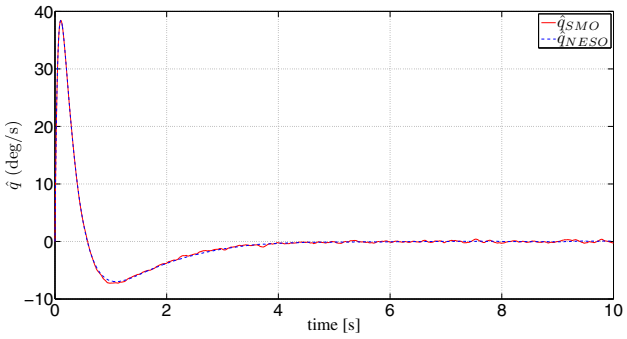


Fig. 14. Response of the pitch rate with SMO or NESO

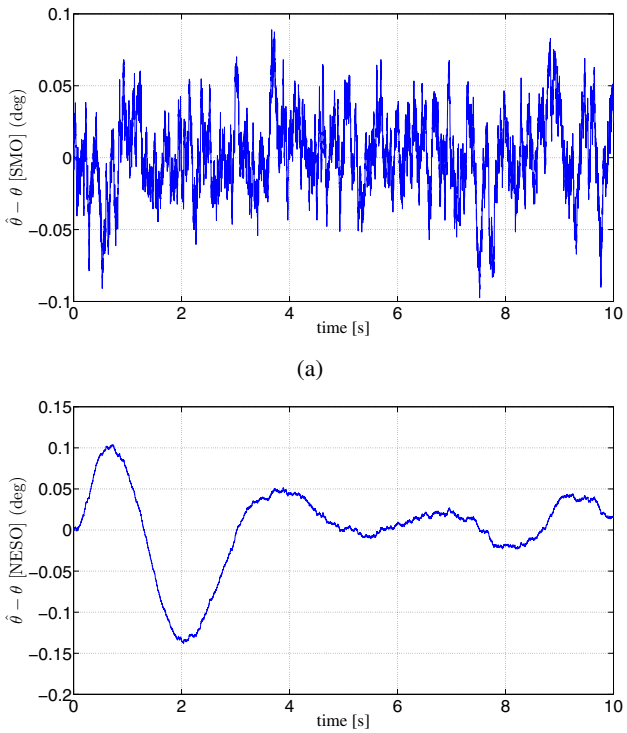


Fig. 15. Estimation errors for pitch angle (a) Estimation error with SMO (b) Estimation error with NESO

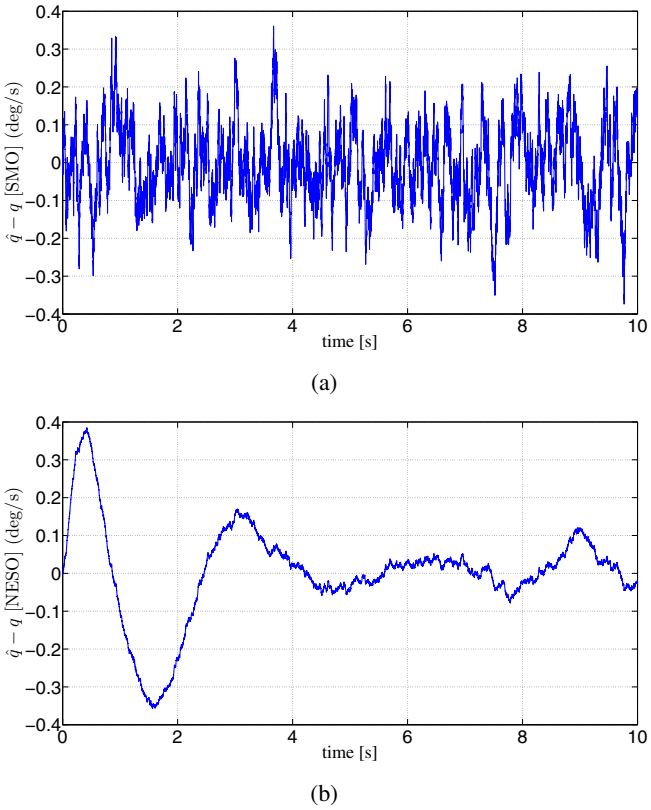


Fig. 16. Estimation errors for pitch rate (a) Estimation error with SMO (b) Estimation error with NESO

## VI. Experimental Results

This section presents the embedded system fixed-wing UAV and the obtained experimental results of the SMO.

We start by presenting the embedded system that has been used in order to test the observers. The embedded system consists of a microprocessor rabbit RCM6000 which reads the data from the Inertial Measurement Unit (IMU), and it also reads the radio signals. The used IMU corresponds with the MicroStrain 3DM-GX1, which give us the Euler angles $(\theta, \psi, \phi)$ and the angular rates $(\dot{\theta}, \dot{\psi}, \dot{\phi})$. In order to estimate the observers, we have taken the Euler angles from the IMU, and then, we have used the angular rates from the IMU in order to compare the estimate results of our observer. The radio control that is used to pilot and to give the autopilot commands is the Futaba T7C (transmitter and receiver). We have used a wireless module in order to obtain all necessary data to compute and to graph the law control signals, this module is a XBee-PRO 802.15.4.

In order to get the altitude, we have used an

Fig. 17. Embedded system on the experimental platform

altimeter and the microcontroller Parallax. This system has been connected to a Rabbit RCM6000. See Figure 17.

Concerning the experimental results of the SMO, we have used the estimated states as feedback signals for a Proportional-Derivative (PD) control law. We do not present the NESO because at this time we have not finished the implementation (tuning) of the algorithm in the embedded microprocessor. The Table II shows the related parameters and constants of the PD controller and SMO.

| | | | | | | |
|---|---|---|---|---|---|---|
| Yaw SMO | $k_{p\psi}$ 5 | $k_{v\psi}$ 1 | $k_1$ 0.02 | $k_2$ 0.1 | $\alpha_1$ 32 | $\alpha_2$ 290 |
| Roll SMO | $k_{p\phi}$ 5 | $k_{v\phi}$ 1 | $k_1$ 0.005 | $k_2$ 0.005 | $\alpha_1$ 38 | $\alpha_2$ 240 |
| Pitch SMO | $k_{ph}$ 10 | $k_{vh}$ 0.1 | $k_1$ 0.01 | $k_2$ 0.001 | $\alpha_1$ 17 | $\alpha_2$ 75 |

TABLE II
EXPERIMENTAL PARAMETERS

### A. Yaw movement

For the experiment in the yaw motion, we fixe a reference angle ($\psi_d$) during the flight of the fixed-wing UAV, and then, the controller must maintain such a reference. The Figure 18 shows the desired yaw angle ($\psi_d$), the yaw response taken from the sensor ($\psi$) and the estimated yaw angle ($\hat{\psi}$).

The yaw rate ($r$) and the estimated yaw rate ($\hat{r}$) are shown in Figure 19.

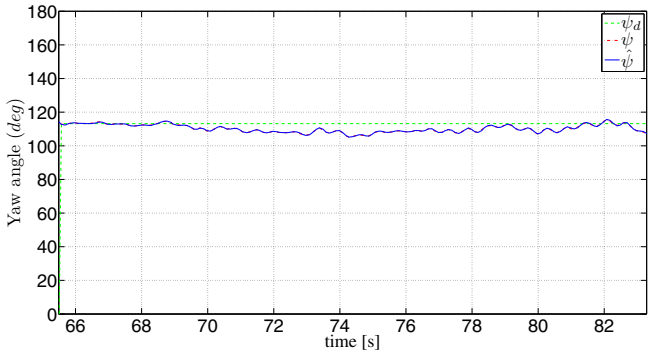


Fig. 18. Estimated yaw angle in the experimental results

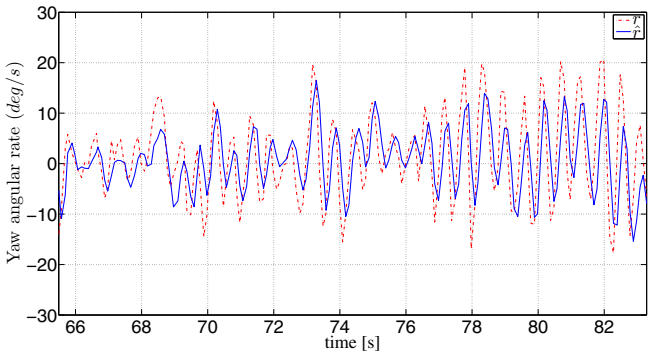


Fig. 19. Estimated yaw rate in the experimental results

In Figure 20, the estimation errors are presented for the yaw motion. The estimation error of yaw angle ($\hat{\psi} - \psi$) can be seen in Figure 20(a) and the estimation error of yaw rate ($\hat{r} - r$) is shown in Figure 20(b).

### B. Roll movement

For this movement, the desired roll angle is fixed in zero degrees ($\phi_d = 0$). The response for this movement can be seen in Figures 21 and 22, which represent the behavior of angle ($\phi$) and the estimated angle of roll ($\hat{\phi}$), in the case of Figure 21, and the response of the roll rate ($p$) in contrast with estimated roll rate ($\hat{p}$) in the Figure 22.

The estimation errors $\hat{\phi} - \phi$ and $\hat{p} - p$ of the experiment results, for the roll motion, are shown in Figure 23.

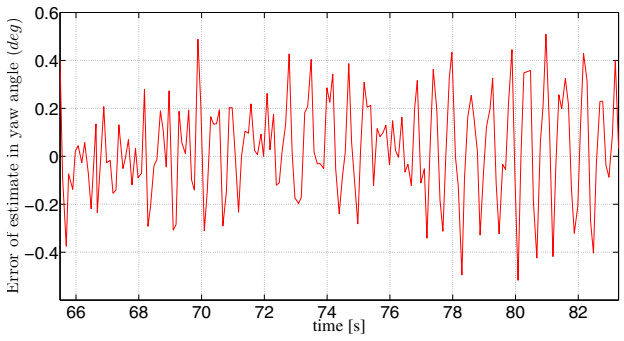


(a)

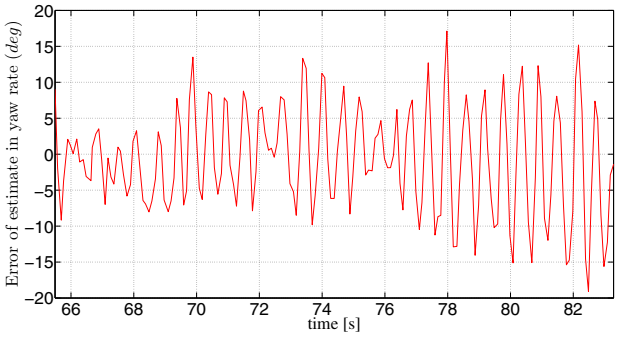


(b)

Fig. 20. Estimation error for yaw in the experimental results (a) Estimation error for the yaw angle (b) Estimation error for the yaw rate

## C. Experimental altitude movement

The goal for this experiment results consist of keeping the fixed-wing UAV on a desired height ($h_d$). The estimated states from SMO are used as feedback states for the PD control law. The Figure 24 shows the desired height ($h_d$) and the measured height ($h$).

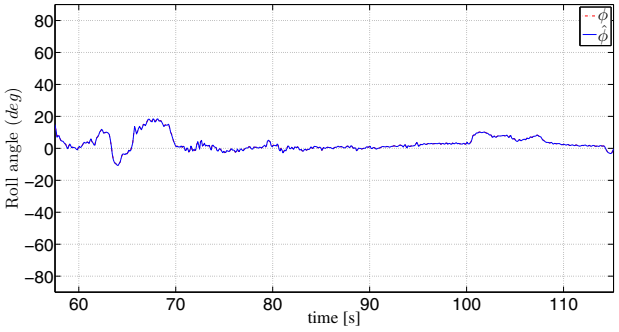


Fig. 21. Estimated roll angle in the experimental results

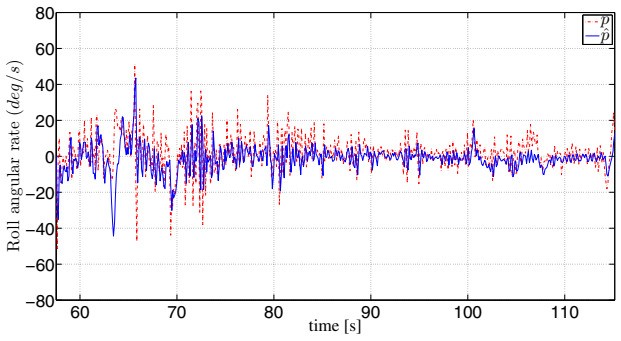


Fig. 22. Estimated roll rate in the experimental results

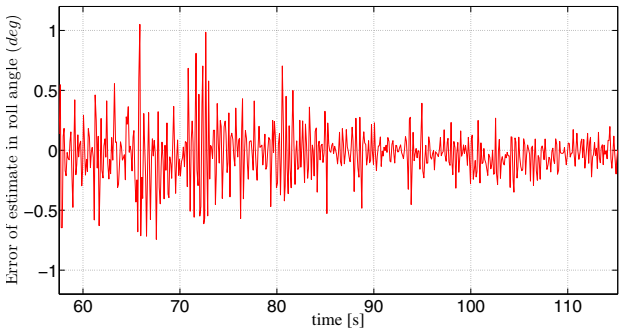


(a)

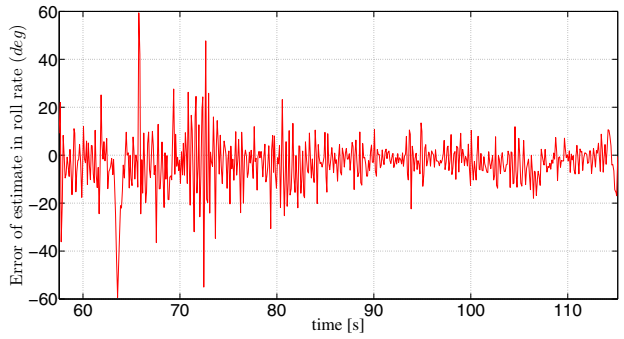


(b)

Fig. 23. Estimation error for roll in the experimental results. (a) Estimation error for the roll angle. (b) Estimation error for the roll rate.

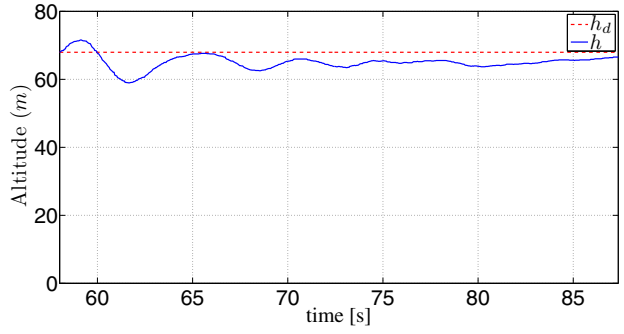


Fig. 24. Altitude motion behaviour, in the experimental results, when applying a PD control law with SMO

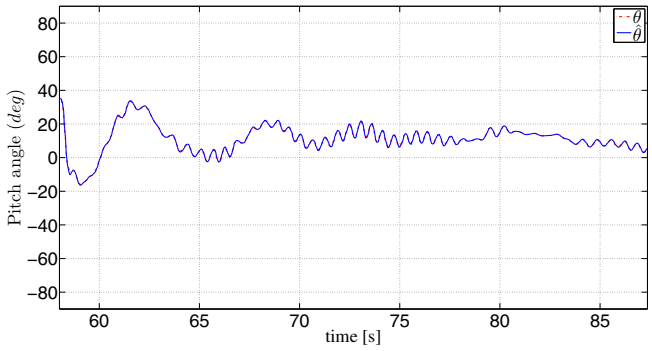


Fig. 25. Estimated pitch angle in the experimental results

The pitch angle behavior, measured by the IMU ($\theta$), and the estimated by the observer ($\hat{\theta}$), can be seen in Figure 25.

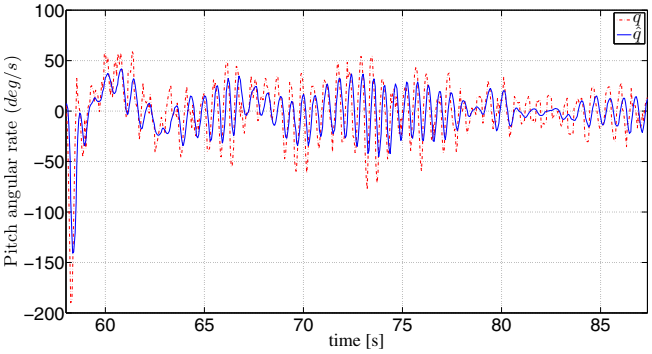


Fig. 26. Estimated pitch rate in the experimental results

The pitch rate ($q$) and the estimated ($\hat{q}$), are shown in Figure 26.

Figure 27 presents the experimental result of the estimation errors $\hat{\theta} - \theta$ and $\hat{q} - q$.

## VII. Conclusions and Future Work

We have designed two observers which are based on the sliding-mode observer and the nonlinear extended state observer. Both have been used to estimate the attitude (pitch, roll, and yaw) and the respective angular rates for a fixed-wing UAV. We have realized a comparative analysis of such observers in order to know what observer has a better performance. Next, we have implemented a proportional-derivative control law with the SMO in order to validate its performance.

In the simulation results, the sliding-mode observer has an acceptable performance for the three

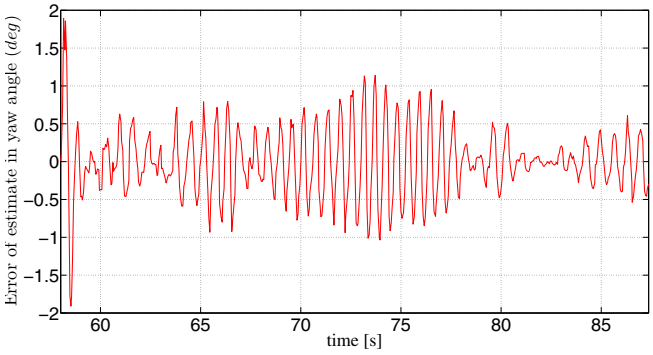


(a) Estimation error for the experimental pitch angle

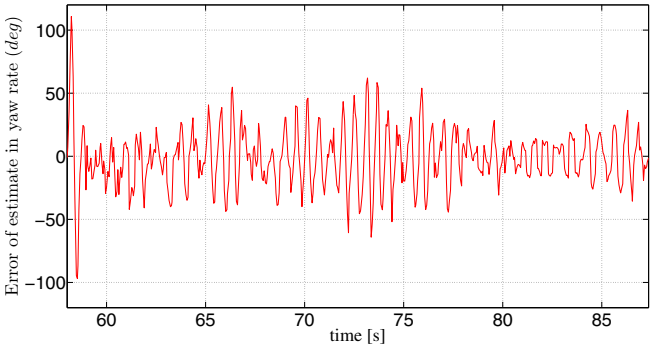


(b) Estimation error for the experimental pitch rate

Fig. 27. Estimation error for pitch in the experimental results (a) Estimation error for pitch angle (b) Estimation error for pitch rate

movements (yaw, roll and altitude). The sliding-mode observer presents a lowed error with respect to the nonlinear extended state observer. This is due to the nonlinear extended state observer does not take into account all the dynamics of the system. We also present some experimental results of the proportional-derivative (PD) control law with the sliding mode observer. The testbed is a radio-controlled airplane. We can observe that the PD control law, with SMO, has a good performance for each one of the three analyzed dynamics, that is, every motion achieves the desired objectives.

Our future work will be focused in the real-time implementation of the nonlinear extended state observer. We will then analyse both observers in real-time conditions.

## References

[1] D. Luenberger. "Observers for multivariable systems". *IEEE Trans. Autom. Control*, vol. 11, pp. 190-197, April 1966.

[2] W. Wang, and Z. Gao. "A Comparison Study of Advanced State Observer Design Techniques". *American Control Conference*, vol. 6, 4590 - 4595, Denver, Colorado, USA, December, 2003.

[3] J. J. E. Slotine, J. K. Hendick, and E. A. Misawa. “On sliding observers for nonlinear systems”. *Journal of Dynamic Systems, Measurement, and Control*, vol. 109, pp. 245-252, 1987.

[4] V. I. Utkin. *Sliding-modes in control optimization*. Book, Springer-Verlag,1992.

[5] R. Sreedhar, B. Fernandez, and G. Y. Masada. “Robust fault detection in nonlinear systems using sliding-mode observers”. *Proceedings of IEEE Conference on Control Applications*, pp 13 - 16, Vancouver, BC., September, 1992.

[6] F. J. J. Hermans and M. B. Zarrop. “Sliding-mode observers for robust sensor monitoring”. *Proceedings of $13^{th}$ IFAC World Congress*, pp. 211-216, San Francisico, USA, 1996.

[7] G. Foo and M. F. Rahman. “Sensorless Sliding-Mode MTPA Control of an IPM Synchronous Motor Drive Using a Sliding-Mode Observer and HF Signal Injection”. *IEEE Transactions on Industrial Electronics*, vol 57, issue 4, pp 1270 - 1278, April 2010.

[8] J. Han. “A class of extended state observers for uncertain systems”. *Control and Decision*, vol.10, No.1, pp: 85-88, 1995. (In Chinese)

[9] Y. Hou, Z. Gao, F. Jiang, and B.T. Boulter. “Active disturbance rejection control for web tension regulation”. *Proceedings of the $40^{th}$ IEEE Conference on Decision and Control*, pp. 4974-4979, Orlando, Florida USA, December, 2001.

[10] Z. Gao, S. Hu, and F. Jiang., “A novel motion control design approach based on active disturbance rejection”. *Proceedings of the $40^{th}$ IEEE Conference on Decision and Control*, pp. 4877-4882, Orlando, Florida USA, December, 2001.

[11] J. Guerrero and R. Lozano, “Flight Formation Control”. *Ed. Wiley*, ISBN: 184-82-1323-9, 2012.

[12] Bernard Etkin and Lloyd Duff Reid, “Dynamics of Flight: Stability and Control”, Third Edition, *Ed. Wiley*, ISBN: 0471034185, 1995.

[13] O. Harkegard and S. T. Glad, “A Backstepping design for Flight Path Angle Control”, *In proceedings of the 39th Conference on Decision and Control*, Sydney, Australia, 12-15 Dic, Page(s):3570 - 3575 vol.4, 2000.

[14] Brian L. Stevens and Frank L. Lewis, “Advances in Unmanned Aerial Vehicles”, *Ed. Jhon Wiley and Sons*, ISBN: 0-471-61397-5, 1992.

[15] M. V. Cook, “Flight Dynamics Principles”, Second edition, *Ed. Elsevier*, ISBN: 978-0-7506-6927-6, 2007.

[16] D. Mclean, “Automatic Flight Control Systems”, *Ed. Prentice hall International*, ISBN: 0-13-054008-0, 1990.

[17] R Kelly, V. Santibáñez., “Control of Robot Manipulators in Joint Space”, *Ed. Springer Verlag*, London Limited U.K., Julio 2005.

[18] Katsuhiko Ogata, “Modern Control Engineering”, *Ed. Prentice Hall*, 2002.